 doi: 10.1111/cpf.12493

PET/CT to detect adverse reactions to metal debris in patients with metal-on-metal hip arthroplasty: an exploratory prospective study

Erik Aro[1,2], Marko Seppänen[2,3,4], Keijo T. Mäkelä[1], Pauliina Luoto[3], Anne Roivainen[3,4] and Hannu T. Aro[1]

[1]Orthopaedic Research Unit, Department of Orthopaedic Surgery and Traumatology, Turku University Hospital and University of Turku, [2]Department of Clinical Physiology and Nuclear Medicine and Turku PET Centre, Turku University Hospital, [3]Turku PET Centre, University of Turku, and [4]Turku PET Centre, Turku University Hospital, Turku, Finland

Summary

Metal-on-metal (MoM) bearings in total hip arthroplasties and hip resurfacing arthroplasties have recently shown a new type of complication: adverse reactions to metal debris (ARMD). ARMD is characterized by local severe inflammation and tissue necrosis leading to implant failures. The gluteal muscle region is important for the patient outcome after revision surgery. This prospective positron emission tomography/computed tomography (PET/CT) study was undertaken to evaluate the characteristics of 2-deoxy-2-[^{18}F]fluoro-D-glucose ([^{18}F]FDG) and [^{68}Ga]Gallium citrate ([^{68}Ga]Citrate) PET/CT in ARMD patients. [^{18}F]FDG and [^{68}Ga]Citrate PET/CT were performed in 18 hip arthroplasty patients: 12 ARMD patients (with 16 MoM hips) and six arthroplasty controls without ARMD. Tracer uptake was evaluated visually, and maximum standardized uptake (SUV_{max}) was measured in the gluteal muscle region. ARMD severity was graded by metal artefact reduction sequence-magnetic resonance imaging (MARS-MRI). Periprosthetic [^{18}F]FDG uptake was observed in 15 of 16 hips, [^{68}Ga]Citrate uptake in three of 16 hips, respectively. The distribution of tracer uptake resembled infection in three hips. In the gluteal muscle region, the SUV_{max} of [^{18}F]FDG was significantly greater in hips with moderate and severe ARMD compared with the controls ($P = 0{\cdot}009$ for [^{18}F]FDG and $P = 0{\cdot}217$ for [^{68}Ga]Citrate). In patients who needed revision surgery, an intraoperative finding of gluteal muscle necrosis was associated with increased local SUV_{max} as detected by preoperative [^{18}F]FDG ($P = 0{\cdot}039$), but not by [^{68}Ga]Citrate ($P = 0{\cdot}301$). In conclusion, the inflammatory reaction to metal debris in hip arthroplasty patients is best visualized with [^{18}F]FDG.

Correspondence
Hannu T. Aro, Orthopaedic Research Unit, Department of Orthopaedic Surgery and Traumatology, Turku University Hospital and University of Turku, Hämeentie 11, Turku 20521, Finland
E-mail: hannu.aro@utu.fi

Accepted for publication
Received 15 March 2017;
accepted 23 November 2017

Key words
adverse reactions to metal debris; hip arthroplasty; magnetic resonance imaging; metal-on-metal hip prosthesis; PET/CT

Introduction

Hip arthroplasty is one of the most successful surgical procedures and is associated with a low prevalence of complications (Learmonth *et al.*, 2007). One of the most critical issues is the selection of articulating bearing surfaces (Rajpura *et al.*, 2014). Metal-on-metal (MoM) bearings have been designed to improve endurance (Bozic *et al.*, 2012). Over 1 million patients worldwide have received MoM bearings, either in the form of hip resurfacing arthroplasty or total hip arthroplasty (THA). Reported complications associated with hip prostheses using MoM bearings have been unexpected (Rising *et al.*, 2012). Compared with alternative types of bearings, hip prostheses with MoM bearings have shown a 2–3-times higher prevalence of failure and ≤30% prevalence of reoperation at 10 years (Murray *et al.*, 2012; Smith *et al.*, 2012). This is well above the current standard; the prevalence of failure should be ≤5% at 10 years. Certain MoM hip prostheses have been withdrawn from the market, whereas those with the best-registered record of survival remain in use.

Early failures of hip prostheses with MoM bearings are due to an entirely new complication: adverse reactions to metal debris (ARMD). This term is used for varying degrees of local tissue reactions in and around the joint: acute and chronic inflammation, necrosis and fibrin deposition (Langton *et al.*, 2011; Mittal *et al.*, 2013). The pathophysiology of ARMD is multifactorial and may be due (at least in part) to a hypersensitivity reaction (Pandit *et al.*, 2008). There are no definitive diagnostic criteria for ARMD.

Metal artefact reduction sequence-magnetic resonance imaging (MARS-MRI) can be used to detect the characteristic diagnostic findings of ARMD, including accumulation of

periprosthetic fluid; cystic and solid areas of tissue necrosis and pseudotumours; oedema and atrophy of muscle; avulsion of gluteal tendons (Anderson *et al.*, 2011; Hauptfleisch *et al.*, 2012). Muscle disease in the gluteal region is: probably secondary to the inflammation associated with ARMD; irreversible; associated with poor outcome in revision surgery (Daniel *et al.*, 2012; Berber *et al.*, 2015). Therefore, patients with large pseudotumours and/or high blood levels of metal ions should be considered for revision surgery or should remain under annual surveillance (Matharu *et al.*, 2016).

The clinical presentation and diagnosis of ARMD can be challenging (Lombardi *et al.*, 2012). Even large pseudotumours of ARMD can be asymptomatic (Williams *et al.*, 2011). The metal particles and ions released from MoM hip joints can affect the immune response to infection (Hosman *et al.*, 2010). Clinically, ARMD may mimic an indolent periprosthetic joint infection (PJI); these two conditions may even coexist (Blumenfeld *et al.*, 2010). Tests to distinguish between ARMD and a PJI are lacking (Della Valle *et al.*, 2010; Wyles *et al.*, 2013).

2-Deoxy-2-[^{18}F]fluoro-D-glucose ([^{18}F]FDG) is the most commonly used tracer for combined positron emission tomography and computed tomography (PET/CT). It is generally used for cancer imaging, but [^{18}F]FDG is also useful in imaging of infection as it is taken up by macrophages in areas of inflammation (Kubota *et al.*, 1992; Zhuang & Alavi, 2002). In 2011, an imaging case report of [^{18}F]FDG PET/CT in a patient with ARMD showed rim-like [^{18}F]FDG uptake in the inflammatory pseudo-capsule, whereas the necrotic interior was almost entirely photopenic (Makis *et al.*, 2011).

Gallium behaves as an *in vivo* iron mimetic that is picked up by sites showing acute/chronic inflammation and tumours (Kumar *et al.*, 2012). While traditional [^{67}Ga]Citrate, a gamma emitter with a half-life of 78 h, required scintigraphic imaging over as long as 72 h, [^{68}Ga]Citrate is a positron emitter with a half-life of just 68 min, allowing rapid sectional imaging using PET/CT (Nanni *et al.*, 2010; Roivainen *et al.*, 2012). [^{68}Ga]Citrate has shown promising results in the detection of skeletal infections and tumours (Mäkinen *et al.*, 2005; Nanni *et al.*, 2010; Behr *et al.*, 2016).

Diagnostic and management algorithms contain no guidance for the use of nuclear imaging modalities in ARMD (Lombardi *et al.*, 2012; Hannemann *et al.*, 2013).

This study was designed as a head-to-head comparison of [^{18}F]FDG and [^{68}Ga]Citrate PET/CT in hip arthroplasty patients suffering from ARMD.

Methods

The present study is registered in the ClinicalTrials.gov database (NCT01970228). The study protocol was approved by the local institutional review board and Ethical Committee of the Hospital District of Southwest Finland, Turku, Finland (decision #81/180/2012). All participants provided written informed consent.

Patients

ARMD patients were recruited from a population of hip arthroplasty patients (n = 2203) who were recalled for safety evaluation of MoM bearings at Turku University Hospital (Turku, Finland). Patients who had symptoms and/or functional impairment were selected to undergo MARS-MRI according to national guidelines. If the MARS-MRI was in keeping with ARMD, the patient was asked to participate in the PET/CT study.

The inclusion criterion was adult hip arthroplasty patients with American Society of Anesthesiology score I–III. The exclusion criteria were any related condition of the index hip which necessitated immediate surgical intervention, such as a septic infection or a periprosthetic fracture.

The selected subjects represented a consecutive sample of eligible patients. This was an exploratory prospective study for which a power analysis was not carried out.

The planned recruitment of ARMD patients (n = 10 and 2 additional patients to replace any withdrawal from the study) was undertaken between October 2012 and May 2013.

Based on the criteria of Reinartz *et al.* (2005), six symptomatic hip arthroplasty patients without ARMD were recruited as controls (four females and two males with a mean age of 66·8 ± 3·2 years) (Fig. 1). There were five controls with unilateral THA and one control with bilateral THA. Five controls had conventional bearings and one had MoM bearings. The time elapsed from their THA to PET/CT was 3·4 ± 2·4 years.

Hip implants of adverse reactions to metal debris patients

All of 12 ARMD patients had MoM bearings in either THA or hip resurfacing arthroplasty. Five patients had unilateral THA and two patients had bilateral THA with cementless femoral stem and acetabular cup components with MoM bearings. The nine hips comprised seven large-diameter M2a-Magnum implants (Biomet, Warsaw, IN, USA) and two Durom Cup implants (Zimmer, Warsaw, IN, USA). Another three patients had unilateral hip resurfacing arthroplasties, and another two patients had bilateral hip resurfacing arthroplasties, all of which were Birmingham hip resurfacing implants (Smith and Nephew, Memphis, TN, USA). The mean time from primary surgery to PET/CT was 6·8 (range, 1·7–10·1) years.

Clinical assessment and screening blood tests

All patients underwent clinical examination and routine imaging of their hips. Local symptoms such as pain were assessed using a questionnaire and visual analogue scale (VAS) of pain. The Western Ontario and McMaster Universities Osteoarthritis Index score (WOMAC) was used to evaluate functional disability on a scale from 0 (asymptomatic) to 100 (extremely

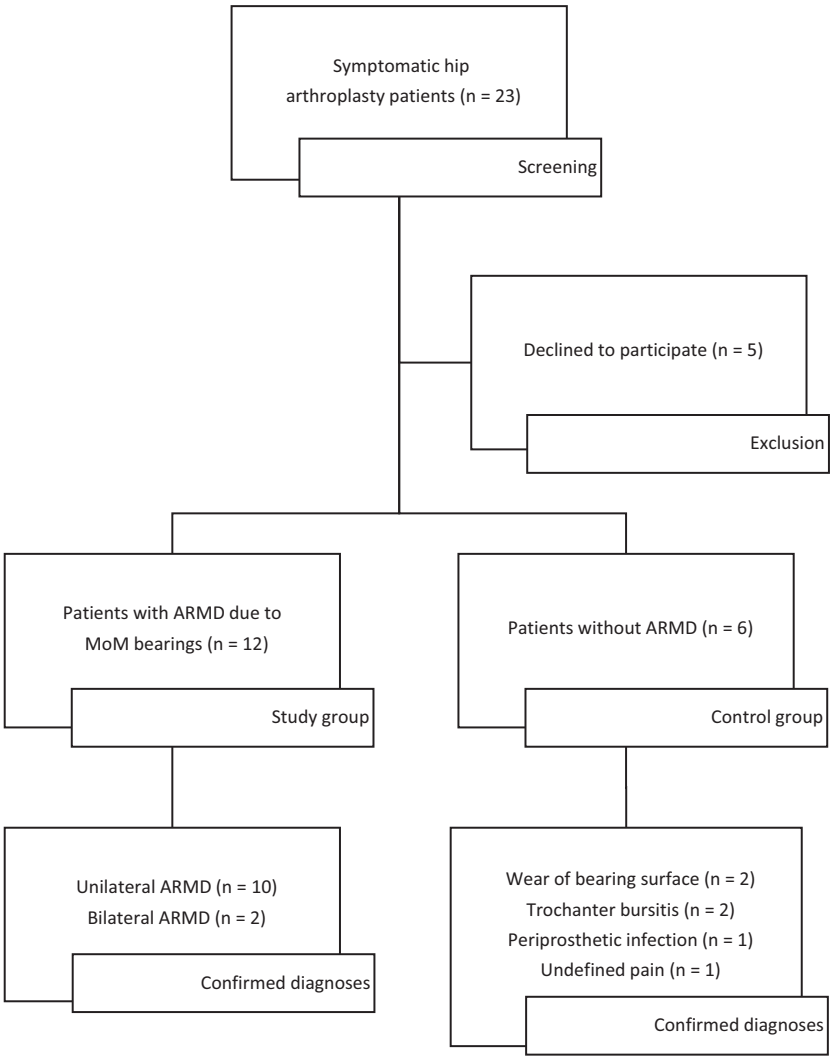

Figure 1 The recruitment process of the study subjects and the final diagnoses.

symptomatic). Patients were excluded for having a PJI by following the current guidelines of the American Academy of Orthopaedic Surgeons (Della Valle *et al.*, 2010), including the measurement of the erythrocyte sedimentation rate (ESR) and C-reactive protein (CRP) and, if indicated, fluid aspiration of the hip joint under fluoroscopy. Serum levels of cobalt and chromium were determined, and the threshold values for unilateral and bilateral hip resurfacing arthroplasties were applied (Van der Straeten *et al.*, 2013).

Metal artefact reduction sequence-magnetic resonance imaging

All patients had a normal glomerular filtration rate. The patients underwent MARS-MRI with contrast medium using 1·5-T scanners and recommended imaging protocols (Hart *et al.*, 2009; Yanny *et al.*, 2012). The severity of ARMD-related changes in periprosthetic soft tissue on MARS-MRI was classified using the grading system described by Anderson *et al.* (2011) (Table 1).

Acquisition of positron emission tomography and computed tomography images

After a 6-h fast, patients were studied by PET/CT. Patients were encouraged to drink water before study commencement. PET/CT (Discovery VCT; General Electric Medical Systems, Milwaukee, WI, USA) was carried out on the same day starting with [^{68}Ga]Citrate PET/CT and followed, 6-h later, with [^{18}F]FDG PET/CT. The Discovery VCT system had a 64-slice CT portion and a PET portion based on crystals of bismuth germanium oxide. The injected radioactivity dose of [^{68}Ga]Citrate was 186 ± 10 MBq, and image acquisition of the hips (10 min per bed position for 1–2 bed positions) began 60 min after injection. The intravenous dose of [^{18}F]FDG was 243 ± 14 MBq. Patients were scanned for 5 min per bed position, and 1–2 bed positions were required to cover the entire hip prosthesis. Imaging began 45 min after injection. Low-dose CT was used for attenuation correction (at settings of 120 kV, ≤80 mAs, and noise index of 25). The radiation-effective dose of the [^{68}Ga]Citrate injection was estimated to

Table 1 Classification for metal-on-metal (MoM) disease on magnetic resonance imaging performed with metal artefact reduction sequences (MARS-MRI) (Anderson *et al.*, 2011).

Grade	Description	Criteria
A	Normal or acceptable	Normal postoperative appearances including seromas and small haematomas
B	Infection	Fluid filled cavity with high signal T2 wall; inflammatory changes in soft tissues, ±bone marrow oedema
C1	Mild MoM disease	Periprosthetic soft-tissue mass with no hyperintense T2W fluid signal or fluid filled periprosthetic cavity; either less than 5 cm maximum diameter
C2	Moderate MoM disease	Periprosthetic soft-tissue mass/fluid filled cavity greater than 5 cm diameter or C1 lesion with either of following: (i) muscle atrophy or oedema in any muscle other than short external rotators or (ii) bone marrow oedema: hyperintense on short tau inversion recovery sequences (STIR)
C3	Severe MoM disease	Any of the following: (i) fluid filled cavity extending through deep fascia, (ii) a tendon avulsion, (iii) intermediate T1W soft-tissue cortical or marrow signal, (iv) fracture

be the same as an effective dose of [^{68}Ga]DOTA-D-Phe^{1}-Try^{3}-Octreotide (i.e., 4·3 mSv). The mean effective dose of the [^{18}F]FDG injection was 4·9 mSv (no authors listed, *Ann IRCP*, 1998; Hartmann *et al.*, 2009). The effective dose of CT to the pelvis was 1·4 mSv.

Analyses of positron emission tomography and computed tomography images

Transaxial, coronal and sagittal images for visual analyses of the data were corrected for dead time, decay and photon attenuation. PET images were reconstructed using a fully three-dimensional maximum-likelihood ordered subset expectation maximization algorithm with two iterations, 28 subsets and a 6·0-mm full-width half-maximum postfilter. The matrix size was 128 × 128 in a 70-cm transaxial field of view, which yielded a pixel size of 5·5 × 5·5 mm. [^{18}F]FDG and [^{68}Ga]Citrate PET/CT images were analysed with an OsiriX PRO workstation (Aycan Medical Systems, Rochester, NY, USA). Non-attenuation-corrected PET images were also analysed.

Qualitative visual analyses of tracer distribution in periprosthetic regions were classified according to the system of (Reinartz *et al.*, 2005), which was developed to evaluate PET images in patients with painful THAs. The descriptive patterns used in this classification were as follows: 1 – no increase in [^{18}F]FDG uptake at the prosthesis–bone interface; 2 – increased uptake of [^{18}F]FDG in the area around the femoral neck; 3 – increased uptake of [^{18}F]FDG in the femoral neck and parts of the prosthesis–bone interface of the acetabular cup and/or proximal stem; 4 – increased uptake of [^{18}F]FDG in the femoral neck and whole prosthesis–bone interface of the acetabular cup and/or in the wide parts of the stem as a sign of mechanical loosening of the prosthesis; 5 – uptake of [^{18}F]FDG in the periprosthetic soft tissue, indicating a PJI. The measurement of the maximum standardized uptake value (SUV_{max}) was focussed on the region of interest (ROI) in the gluteal muscle region. A fixed-dimension circular ROI (diameter, 1·5 cm) was positioned manually over the region in the gluteal muscles with the highest uptake, and the SUV_{max} was calculated.

Follow-up for revision surgery

The treating orthopaedic surgeons were blinded to the SUV_{max} values of the tracers. During the follow-up (≥3 years after imaging and ≥5 years after implantation), seven patients underwent revision surgery. The time elapsed from PET/CT to revision surgery varied between 1 and 46 months (median 4 months). Four of seven (57%) revision surgical procedures had an intraoperative finding (microscopic or macroscopic) of necrosis in the gluteal muscles (Table 2). Intraoperative tissue samples were submitted for microbiological and histopathological analyses. All samples were negative for bacterial infection. Removed implant components were also negative for the enhanced exclusion of biofilm-type infection using ultrasonic vibration (Gomez & Patel, 2011).

Statistical analyses

Statistical analyses were undertaken using Prism v7.01 (GraphPad, La Jolla, CA, USA). The SUV_{max} data, expressed as the mean ± standard deviation (SD), were tested for normality using the Shapiro–Wilk test. For analyses of data with a normal distribution, the independent-sample *t*-test was applied to test the significance of differences between two groups. The nonparametric Kruskal–Wallis test was applied for the comparison of two subgroups (no/mild and moderate/severe) of ARMD patients with the controls. A P value<0·05 (two-sided) was considered significant.

Results

All 12 recruited patients with ARMD (Table 2) completed the study. The most frequently reported symptoms were 'pain upon exercise' (11/12, 92%), 'morning stiffness' (11/12, 92%), 'night pain' (8/12, 67%), 'night sweats' (7/12, 58%), 'sensation of heat' (6/12, 50%), 'chills' (4/12, 33%), 'fever'

Table 2 Characteristics of the ARMD patients (n = 12).

Characteristic	Value[a]
Age (years)	64·6 ± 5·5
Gender	
Male	7 (58%)
Female	5 (42%)
Laterality of hip arthroplasty	
Right hip	5 (42%)
Left hip	3 (25%)
Bilateral	4 (33%)
Type of hip arthroplasty with MoM bearings	
Total hip arthroplasty	9 (56%)
Unilateral	5
Bilateral	4
Hip resurfacing arthroplasty	7 (44%)
Unilateral	3
Bilateral	4
Time elapsed from operation to PET/CT (years)	6·8 ± 2·0
VAS[b] (0–10)	4·7 ± 2·5
WOMAC[c] score (0–100)	32 ± 14
CRP and/or ESR values	
Above cut-off values[d]	3 (25%)
Below cut-off values	9 (75%)
Serum levels of cobalt and chromium	
Above the recommend threshold values[e]	10 (83%)
Below the recommend threshold values	2 (17%)
Revision surgery in follow-up	
Yes	7 (44%)
Intraoperative gluteal necrosis	4 (25%)
No intraoperative gluteal necrosis	3 (19%)
No	9 (56%)

[a]Values are means ± SD or n (%).
[b]Visual analogue scale of pain from 0 (no pain) to 10 (worst imaginable pain).
[c]The Western Ontario and McMaster Universities Osteoarthritis Index score to evaluate functional disability on a scale from 0 (asymptomatic) to 100 (extremely symptomatic).
[d]The cut-off values 10 mg l^{-1} for CRP and 30 mm h^{-1} for ESR (Schinsky *et al.*, 2008)
[e]The threshold values of 4·6 μg l^{-1} for chromium and 4·0 μg l^{-1} for cobalt in unilateral hip resurfacing arthroplasty and 7·4 μg l^{-1} for chromium and 5·0 μg l^{-1} for cobalt for bilateral hip resurfacing arthroplasty (Van der Straeten *et al.*, 2013).

(4/12, 33%) and 'mechanical sensations' (3/12, 25%). Three patients had increased CRP levels (range, 16–21 mg l^{-1}) and/or increased ESR values (range, 32–46 mm h^{-1}). As recommended (Della Valle *et al.*, 2010), these patients underwent fluid aspiration of the hip joint to rule out infection. All cultures of joint fluid were negative. Ten patients had serum levels of cobalt and chromium that exceeded threshold values (Van der Straeten *et al.*, 2013).

Eight ARMD patients had a unilateral MoM hip and four had bilateral MoM hips. Thus, the 12 patients had 16 MoM hips. MARS-MRI images (Table 3) revealed that all 12 patients suffered from ARMD in at least one hip. Of the 16 MoM hips, 14 were affected by ARMD. In four patients with bilateral MoM hips, two of these cases had ARMD bilaterally and two had ARMD unilaterally. Twelve (75%) hips showed moderate (grade C2) or severe (grade C3) ARMD. No hips had MARS-MRI findings that suggested infection (grade B). Eight MoM hips had thin-walled fluid collections, and six MoM hips had thick-walled and cystic areas of inflammation that formed pseudotumours.

Table 3 Metal artefact reduction sequence-magnetic resonance imaging (MARS-MRI) results and positron emission tomography combined with computed tomography (PET/CT) tracer distribution (n = 16).

Characteristic	Value
ARMD classification[a] (MARS-MRI)	
Grade A (normal)	2 (13%)
Grade B (infection)	0 (0%)
Grade C1 (mild ARMD)	2 (13%)
Grade C2 (moderate ARMD)	9 (56%)
Grade C3 (severe ARMD)	3 (19%)
Thin-walled cystic fluid collections	8 (50%)
Thick-walled cystic pseudotumours	6 (38%)
[^{18}F]FDG periprosthetic distribution pattern[b]	
Pattern 1	1 (6%)
Pattern 2	7 (44%)
Pattern 3	5 (31%)
Pattern 4	0 (0%)
Pattern 5	3 (19%)
[^{68}Ga]Citrate periprosthetic distribution pattern[b]	
Pattern 1	13 (81%)
Pattern 2	0 (0%)
Pattern 3	1 (6%)
Pattern 4	0 (0%)
Pattern 5	2 (12%)

Values are n (%).
[a]Classification according to Anderson *et al.* (2011).
[b]Classification according to Reinartz *et al.* (2005).

[^{18}F]FDG positron emission tomography and computed tomography

Table 3 shows the pattern of [^{18}F]FDG uptake observed in the MoM hips of patients with ARMD. Only one hip did not show any [^{18}F]FDG uptake in the periprosthetic area. The most common finding in 12 (75%) of 16 hips was tracer uptake in the area of the femoral neck alone (pattern 2) or tracer uptake in the femoral neck and parts of the prosthesis–bone interface (pattern 3). The distribution of [^{18}F]FDG uptake in the periprosthetic soft tissues (especially in the gluteal muscles) resembled a pattern seen typically in infection of three (19%) hips (Fig. 2a). These accumulations were also verified on non-attenuation-corrected images, and only one patient was regarded as showing false-positive tracer uptake due to CT-based attenuation correction artefact in soft tissues.

In the gluteal muscle region, the SUV_{max} values of [^{18}F]FDG were significantly greater in hips with moderate or severe ARMD compared with hips of the controls ($P = 0·009$) (Fig. 3). Patients who had necrosis in the gluteal muscles

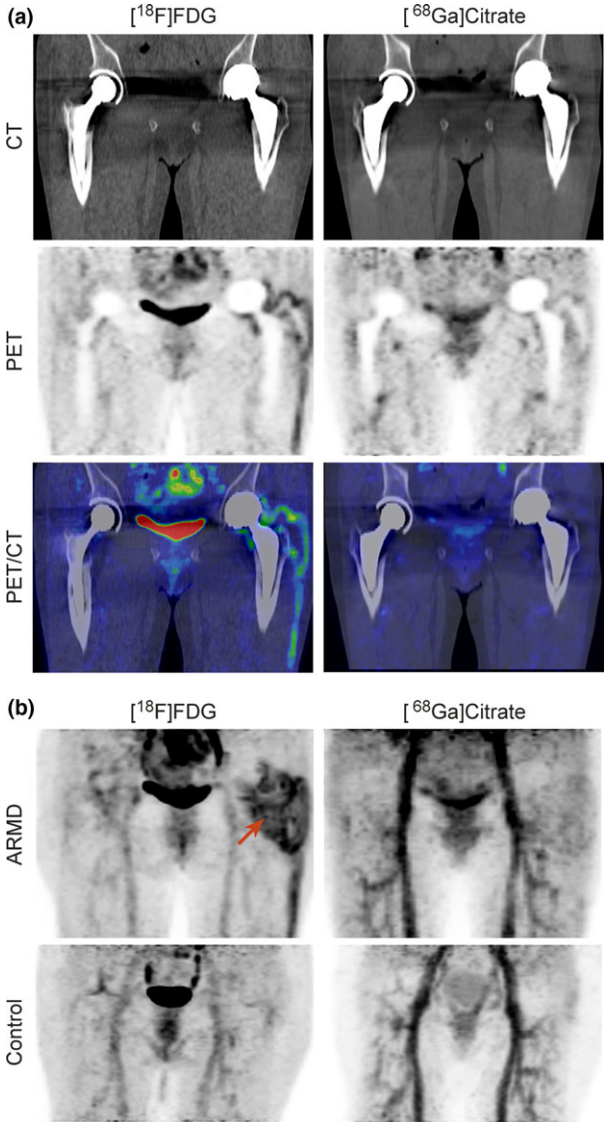

Figure 2 (a) PET/CT imaging of a 67-year-old woman with THAs with bilateral moderate ARMD due MoM bearings. The patient had symptoms only on the left hip. The periprosthetic distribution patterns of [^{18}F]FDG and [^{68}Ga]Citrate were abnormal in the left hip, resembling periprosthetic infection (pattern 5 according to the Reinartz *et al.* classification). The patient had normal CRP and ESR. Synovial fluid cultures of the hip were negative. (b) The comparison of maximum intensity projection (MIP) images of the patient in panel a and a representative patient of the control group. Marked periprosthetic tracer uptake in the left hip of the ARMD patient (red arrow for [^{18}F]FDG). The control, a 69-year-old woman with bilateral THAs with ceramic-ceramics bearings, had unexplained pain in the left hip. The hip showed normal findings in [^{18}F]FDG and [^{68}Ga]Citrate scans.

upon revision surgery showed significantly ($P = 0{\cdot}039$) greater SUV_{max} values of [^{18}F]FDG compared with patients who had no necrosis in the gluteal muscles (Fig. 4). There was no statistically significance ($P = 0{\cdot}164$) in SUV_{max} of [^{18}F]FDG between patients who needed revision surgery within the follow-up period ($n = 7$) and patients who did not ($n = 5$) ($3{\cdot}43 \pm 1{\cdot}75$ and $2{\cdot}38 \pm 1{\cdot}11$, respectively).

[^{68}Ga]Citrate positron emission tomography and computed tomography

The visually interpreted uptake of [^{68}Ga]Citrate remained negative (pattern 1) in 13 (81%) of 16 hips (Table 3). Three hips with increased uptake of [^{68}Ga]Citrate (pattern 3 or 5) were found in the same three patients who showed a pattern of [^{18}F]FDG uptake that suggested infection (pattern 5).

In the gluteal muscle region, the SUV_{max} values of [^{68}Ga]Citrate were not significantly different in hips with moderate or severe ARMD than in the control hips ($P = 0{\cdot}217$) (Fig. 3). Patients who needed revision surgery during the follow-up did not show a significantly increased SUV_{max} value of [^{68}Ga]Citrate compared with those who did not need intervention ($1{\cdot}64 \pm 0{\cdot}58$ versus $1{\cdot}25 \pm 0{\cdot}36$, $P = 0{\cdot}116$). The SUV_{max} values of [^{68}Ga]Citrate were not significantly different in patients with an intraoperative finding of gluteal muscle necrosis compared with patients with no necrosis of the gluteal muscles ($P = 0{\cdot}301$) or who did not need revision surgery (Fig. 4).

[^{18}F]FDG and [^{68}Ga]Citrate positron emission tomography and computed tomography of control hip arthroplasty patients

The confirmed diagnoses of the controls are shown in Fig. 1. Two controls had increased CRP and/or ESR values above the cut-off values. Four controls underwent fluid aspiration of the hip joint due to the suspicion of a PJI. Eventually, only one patient had positive culture of the synovial fluid. [^{68}Ga]Citrate PET/CT correctly (pattern 3 according to the Reinartz *et al.* classification) identified this single case of a low-grade PJI caused by *Staphylococcus epidermidis*, which was associated with normal levels of CRP and ESR. The only control patient with MoM bearings had recurrent skin reactions in the region of the surgical scar and underwent extensive studies (bone scintigraphy, leucocyte scan, MARS-MRI, repeated fluid aspirations of the hip joint and skin biopsies) which ruled out periprosthetic infection, mechanical loosening and ARMD.

Five controls without infection or mechanical loosening showed a normal pattern of tracer uptake in the periprosthetic region (pattern 1 according to the Reinartz *et al.* classification) upon [^{18}F]FDG and [^{68}Ga]Citrate PET/CT (Fig. 2b). Two of these cases had slight uptake of [^{18}F]FDG over the trochanter major as a sign of local bursitis.

The controls, including the patient with low-grade PJI, showed low uptake in the gluteal region. The SUV_{max} values of [^{18}F]FDG and [^{68}Ga]Citrate were $1{\cdot}18 \pm 0{\cdot}21$ and $1{\cdot}25 \pm 0{\cdot}35$, respectively (Fig. 3).

Discussion

The present study was designed to characterize [^{18}F]FDG and [^{68}Ga]Citrate PET/CT findings in hip arthroplasty patients who suffered ARMD due to MoM bearings. We found

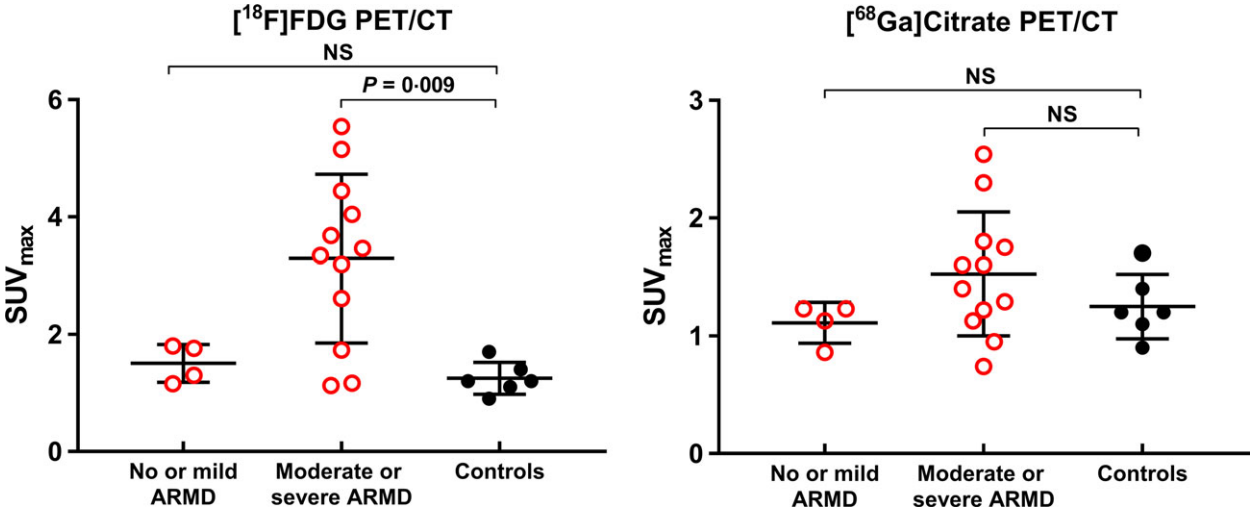

Figure 3 Hips with moderate or severe adverse reactions to metal debris (ARMD) showed high [^{18}F]FDG uptake in the gluteal muscle region compared with the control hips. The corresponding differences in the SUV_{max} values of [^{68}Ga]Citrate were not statistically significant. The dots represent the SUV_{max} values of individual hips, and the bars represent the mean values ± SD.

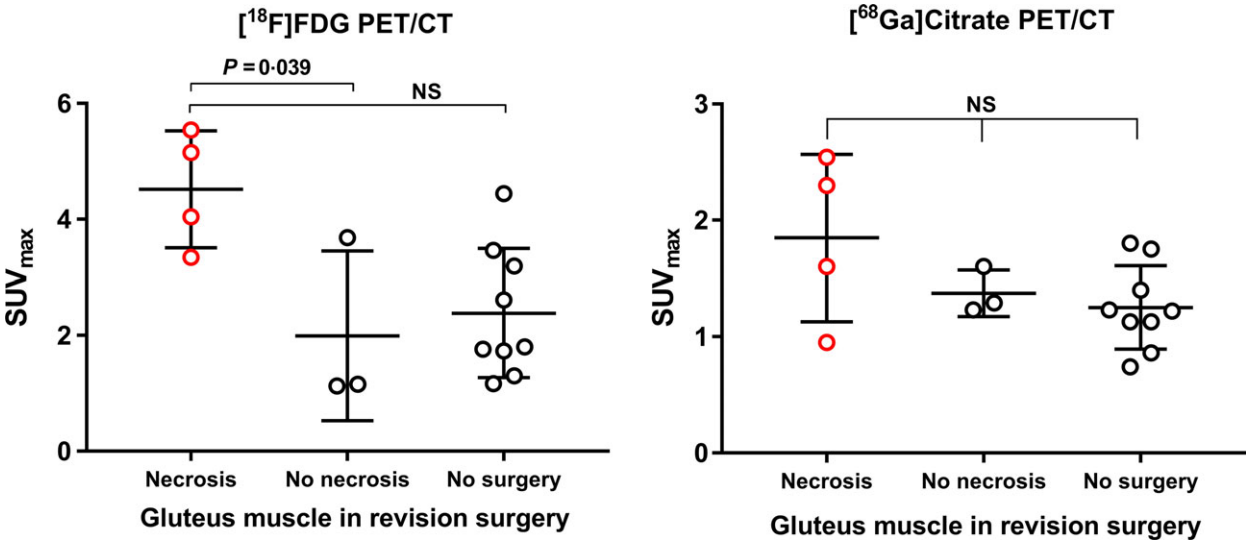

Figure 4 Hips with a surgical finding of gluteal muscle necrosis showed significantly greater local [^{18}F]FDG uptake compared with hips without gluteal muscle necrosis or with no need for revision surgery during the follow-up period. With [^{68}Ga]Citrate imaging, no corresponding differences were found between the three groups of patients. The dots represent the SUV_{max} values of individual hips, and the bars represent the mean values ± SD.

significantly increased uptake of [^{18}F]FDG in the gluteal muscle region in patients with moderate or severe ARMD. The pattern of tracer distribution mimicked infection in three hips. Such cases suggest that the scans may not be able to exclude a PJI in ARMD with severe inflammation and necrosis.

The selection of the gluteal muscle region for the measurement of SUV_{max} was based on clinical relevance. The hip abductors are critical for the normal function and stability of the joint after hip arthroplasty. The gluteal muscles and tendons are affected frequently by the metal-wear debris of ARMD and cause functional deficits (Hosman *et al.*, 2010) and a high prevalence of complications upon revision surgery (Grammatopolous *et al.*, 2009). Therefore, screening of ARMD patients should accurately detect changes in the gluteal muscles and help to identify patients who need immediate surgical intervention (Berber *et al.*, 2015): [^{18}F]FDG PET/CT may fulfil this requirement.

The increased uptake of [^{18}F]FDG in hips with moderate or severe ARMD was likely related to the extent of aseptic, necrotizing inflammation. Thus, [^{18}F]FDG might be useful for monitoring ARMD activity, along with the information provided by MARS-MRI. Treatment decisions (i.e., to carry out or not carry out revision surgery) are difficult in ARMD cases (Matharu *et al.*, 2016). Patients are also hesitant to have

revision surgery if they are asymptomatic. Further studies are required to clarify if measurement of the local uptake of [^{18}F]FDG in the gluteal region could be used to identify patients who are in need of timely revision surgery before irreversible damage to the gluteal muscles occurs.

Only one hip with ARMD did not show any [^{18}F]FDG accumulation. Likewise, there was no uptake of [^{68}Ga]Citrate. This patient presented with only mild symptoms and serum levels of cobalt and chromium that were not increased. However, MARS-MRI showed moderate ARMD with a collection of periprosthetic fluid of maximum diameter of 7 cm. Muscle atrophy was not evident. During a follow-up of 9·5 years after the hip arthroplasty, the symptoms have not worsened and the patient has not been scheduled for revision surgery. In this patient, the lack of tracer uptake could be interpreted as a sign of stable ARMD without major inflammation in the periprosthetic area.

As a tracer that could be employed for diagnosing infection sites, [^{68}Ga]Citrate gave no extra value to the imaging of ARMD patients compared with [^{18}F]FDG. Further studies with [^{68}Ga]Citrate in ARMD patients do not seem to be warranted. However, the present study does not exclude the potential value of [^{68}Ga]Citrate PET/CT for the detection of PJIs in patients without ARMD.

Our study had three main limitations. First, the small study cohort limited the interpretation of the results. This was the first study PET/CT study conducted on ARMD patients, and the planned number of participants was limited due to ethical reasons. The difficulties in recruitment of the planned controls reflected the low prevalence of complications. The current prevalence of revision for mechanical loosening is only 1·4%, and the prevalence of infection in THA patients is 0·5% (Hailer *et al.*, 2015). Second, PET studies of arthroplasty patients (Reinartz *et al.*, 2005; Basu *et al.*, 2014) have used single-modality PET, whereas we applied PET/CT with potential problems due to metal artefacts. Third, we had no readily available reference to interpret the unique uptake of tracer in patients with ARMD. We adopted the Reinartz classification (Reinartz *et al.*, 2005) for the qualitative visual analyses of tracer distribution in periprosthetic areas, which were developed originally for the differentiation of periprosthetic infection and mechanical loosening. This system was not sufficient to describe the characteristic distribution of tracer uptake in ARMD patients, and we chose measurement of the SUV_{max} value of the gluteal muscle region as an additional parameter. SUV_{max} measurements of tracer uptake were undertaken at a distance from the metal components. There was no major uptake of the tracers in the gluteal muscle region in the control patients.

Conclusions

There are four main conclusions to this study. First, the inflammatory pathophysiology of moderate and severe ARMD leads to the high uptake of [^{18}F]FDG in the periprosthetic area. Second, an intraoperative finding of necrosis of the gluteal muscles upon revision surgery was associated with a local increase in [^{18}F]FDG uptake. Third, ARMD patients may show patterns of [^{18}F]FDG and [^{68}Ga]Citrate uptake that are indistinguishable from infection. Lastly, [^{18}F]FDG appears to be sufficient in PET/CT of hip arthroplasty patients with ARMD because there were no cases in which [^{68}Ga]Citrate uptake showed a feature that [^{18}F]FDG did not.

Further prospective studies are needed to examine the value of [^{68}Ga]Citrate PET/CT in the detection of periprosthetic joint infections in arthroplasty patients without ARMD.

Acknowledgments

The authors thank Satu Honkala and Mika Junnila (Turku University Hospital) for their assistance in patient recruitment, Tuula Tolvanen and Nina Savisto (Turku PET Centre) for their assistance in carrying out PET/CT and Timo Kattelus (Turku PET Centre) for helping in preparation the figure of PET images.

Compliance with ethical standards

The study protocol was approved by our institutional review board.

Conflict of interest statement

The authors declare that they have no conflict of interest.

Funding

This study was funded by the Sigrid Jusélius Foundation.

References

Anderson H, Toms AP, Cahir JG, *et al.* Grading the severity of soft tissue changes associated with metal-on-metal hip replacements: reliability of an MR grading system. *Skeletal Radiol* (2011); **40**: 303–307.

Basu S, Kwee TC, Saboury B, *et al.* FDG PET for diagnosing infection in hip and knee prostheses: prospective study in 221 prostheses and subgroup comparison with combined (111)In-labeled leukocyte/(99m)Tc-sulfur colloid bone marrow imaging in 88 prostheses. *Clin Nucl Med* (2014); **39**: 609–615.

Behr SC, Aggarwal R, Seo Y, *et al.* A feasibility study showing [^{68}Ga]citrate PET detects prostate cancer. *Mol Imaging Biol* (2016); **18**: 946–951.

Berber R, Khoo M, Cook E, *et al.* Muscle atrophy and metal-on-metal hip implants: a serial MRI study of 74 hips. *Acta Orthop* (2015); **86**: 351–357.

Blumenfeld TJ, Bargar WL, Campbell PA. A painful metal-on-metal total hip arthroplasty: a diagnostic dilemma. *J Arthroplasty* (2010); **25**: 1168.e1-4.

Bozic KJ, Browne J, Dangles CJ, *et al.* Modern metal-on-metal hip implants. *J Am Acad Orthop Surg* (2012); **20**: 402–406.

Daniel J, Holland J, Quigley L, *et al.* Pseudotumors associated with total hip arthroplasty. *J Bone Joint Surg Am* (2012); **94**: 86–93.

Della Valle C, Parvizi J, Bauer TW, *et al.* American Academy of Orthopaedic Surgeons. Diagnosis of periprosthetic joint infections of the hip and knee. *J Am Acad Orthop Surg* (2010); **18**: 760–770.

Gomez E, Patel R. Laboratory diagnosis of prosthetic joint infection, part II. *Clin Microbiol Newsletter* (2011); **33**: 63–70.

Grammatopolous G, Pandit H, Kwon YM, *et al.* Hip resurfacings revised for inflammatory pseudotumour have a poor outcome. *J Bone Joint Surg Br* (2009); **91**: 1019–1024.

Hailer NP, Lazarinis S, Mäkelä KT, *et al.* Hydroxyapatite coating does not improve uncemented stem survival after total hip arthroplasty!. *Acta Orthop* (2015); **86**: 18–25.

Hannemann F, Hartmann A, Schmitt J, *et al.* European multidisciplinary consensus statement on the use and monitoring of metal-on-metal bearings for total hip replacement and hip resurfacing. *Orthop Traumatol Surg Res* (2013); **99**: 263–271.

Hart AJ, Sabah S, Henckel J, *et al.* The painful metal-on-metal hip resurfacing. *J Bone Joint Surg Br* (2009); **91**: 738–744.

Hartmann H, Zöphel K, Freudenberg R, *et al.* Radiation exposure of patients during ^{68}Ga-DOTATOC PET/CT examinations. *Nuklearmedizin* (2009); **48**: 201–207.

Hauptfleisch J, Pandit H, Grammatopoulos G, *et al.* A MRI classification of periprosthetic soft tissue masses (pseudotumours) associated with metal-on-metal resurfacing hip arthroplasty. *Skeletal Radiol* (2012); **41**: 149–155.

Hosman AH, van der Mei HC, Bulstra SK, *et al.* Effects of metal-on-metal wear on the host immune system and infection in hip arthroplasty. *Acta Orthop* (2010); **81**: 526–534.

Kubota R, Yamada S, Kubota K, *et al.* Intratumoral distribution of fluorine-18-fluorodeoxyglucose in vivo: high accumulation in macrophages and granulation tissues studied by microautoradiography. *J Nucl Med* (1992); **33**: 1972–1980.

Kumar V, Boddeti DK, Evans SG, *et al.* (68) Ga-Citrate-PET for diagnostic imaging of infection in rats and for intra-abdominal infection in a patient. *Curr Radiopharm* (2012); **5**: 71–75.

Langton DJ, Joyce TJ, Jameson SS, *et al.* Adverse reaction to metal debris following hip resurfacing: the influence of component type, orientation and volumetric wear. *J Bone Joint Surg Br* (2011); **93**: 164–171.

Learmonth ID, Young C, Rorabeck C. The operation of the century: total hip replacement. *Lancet* (2007); **370**: 1508–1519.

Lombardi AV Jr, Barrack RL, Berend KR, *et al.* The Hip Society: algorithmic approach to diagnosis and management of metal-on-metal arthroplasty. *J Bone Joint Surg Br* (2012); **94**: 14–18.

Mäkinen TJ, Lankinen P, Pöyhönen T, *et al.* Comparison of ^{18}F-FDG and ^{68}Ga PET imaging in the assessment of experimental osteomyelitis due to *Staphylococcus aureus*. *Eur J Nucl Med Mol Imaging* (2005); **32**: 1259–1268.

Makis W, Rush C, Abikhzer G. Necrotic pseudotumor caused by a metal-on-metal total hip prosthesis: imaging characteristics on (18)F-FDG PET/CT and correlative imaging. *Skeletal Radiol* (2011); **40**: 773–777.

Matharu GS, Ostlere SJ, Pandit HG, *et al.* What is the natural history of asymptomatic pseudotumours in metal-on-metal hip resurfacing patients? *Hip Int* (2016); **26**: 522–530.

Mittal S, Revell M, Barone F, *et al.* Lymphoid aggregates that resemble tertiary lymphoid organs define a specific pathological subset in metal-on-metal hip replacements. *PLoS ONE* (2013); **8**: e63470.

Murray DW, Grammatopoulos G, Pandit H, *et al.* The ten-year survival of the Birmingham hip resurfacing: an independent series. *J Bone Joint Surg Br* (2012); **94**: 1180–1186.

Nanni C, Errani C, Boriani L, *et al.* ^{68}Ga-citrate PET/CT for evaluating patients with infections of the bone: preliminary results. *J Nucl Med* (2010); **51**: 1932–1936.

No authors listed: International Commission on Radiological Protection. ICRP Publication 80. Recalculated dose data for 19 frequently used radiopharmaceuticals from ICRP Publication 53. *Ann ICRP* (1998); **28**: 47–83.

Pandit H, Glyn-Jones S, McLardy-Smith P, *et al.* Pseudotumours associated with metal-on-metal hip resurfacings. *J Bone Joint Surg Br* (2008); **90**: 847–851.

Rajpura A, Kendoff D, Board TN. The current state of bearing surfaces in total hip replacement. *Bone Joint J* (2014); **96-B**: 147–156.

Reinartz P, Mumme T, Hermanns B, *et al.* Radionuclide imaging of the painful hip arthroplasty: positron-emission tomography versus triple-phase bone scanning. *J Bone Joint Surg Br* (2005); **87**: 465–470.

Rising JP, Reynolds IS, Sedrakyan A. Delays and difficulties in assessing metal-on-metal hip implants. *N Engl J Med* (2012); **367**: e1.

Roivainen A, Jalkanen S, Nanni C. Gallium-labelled peptides for imaging of inflammation. *Eur J Nucl Med Mol Imaging* (2012); **39**: 68–77.

Schinsky MF, Della Valle CJ, Sporer SM, *et al.* Perioperative testing for joint infection in patients undergoing revision total hip arthroplasty. *J Bone Joint Surg Am* (2008); **90**: 1869–1875.

Smith AJ, Dieppe P, Vernon K, *et al.* National Joint Registry of England and Wales: failure rates of stemmed metal-on-metal hip replacements: Analysis of data from the National Joint Registry of England and Wales. *Lancet* (2012); **379**: 1199–1204.

Van der Straeten C, Grammatopoulos G, Gill HS, *et al.* The 2012 Otto Aufranc Award: the interpretation of metal ion levels in unilateral and bilateral hip resurfacing. *Clin Orthop Relat Res* (2013); **471**: 377–385.

Williams DH, Greidanus NV, Masri BA, *et al.* Prevalence of pseudotumor in asymptomatic patients after metal-on-metal hip arthroplasty. *J Bone Joint Surg Am* (2011); **93**: 2164–2171.

Wyles CC, Larson DR, Houdek MT, *et al.* Utility of synovial fluid aspirations in failed metal-on-metal total hip arthroplasty. *J Arthroplasty* (2013); **28**: 818–823.

Yanny S, Cahir JG, Barker T, *et al.* MRI of aseptic lymphocytic vasculitis-associated lesions in metal-on-metal hip replacements. *AJR Am J Roentgenol* (2012); **198**: 1394–1402.

Zhuang H, Alavi A. 18-fluorodeoxyglucose positron emission tomographic imaging in the detection and monitoring of infection and inflammation. *Semin Nucl Med* (2002); **32**: 47–59.